International Symposium
On Turbulence and Shear Flow
Phenomena (TSFP-8)
August 28 - 30, 2013 Poitiers, France

INVERSE MAGNUS EFFECT ON A ROTATING SPHERE

Jooha Kim
School of Mechanical and Aerospace Engineering
Seoul National University
Seoul 151-744, Korea
k-juha01@snu.ac.kr

Hyungmin Park
School of Mechanical and Aerospace Engineering
Seoul National University
Seoul 151-744, Korea
hminpark@snu.ac.kr

Haecheon Choi
School of Mechanical and Aerospace Engineering
Seoul National University
Seoul 151-744, Korea
choi@snu.ac.kr

Jung Yul Yoo
School of Mechanical and Aerospace Engineering
Seoul National University
Seoul 151-744, Korea
jyyoo@snu.ac.kr

ABSTRACT

For a rotating sphere or cylinder, the lift coefficients become negative at some specific Reynolds numbers Re and spin ratios α (ratio of surface velocity to the free-stream velocity), called inverse Magnus effect. In the present study, the inverse Magnus effect on a rotating sphere is experimentally investigated at $Re = 0.6 \times 10^5 - 1.8 \times 10^5$, based on the free-stream velocity U_0 and sphere diameter d. By varying the spin ratio from 0 (no spin) to 1.7, we measure the lift, drag, and velocity field behind the rotating sphere. At a given Re, the lift force is positive, negative and then positive again with increasing spin ratio. At higher Reynolds number, the rapid decrease of the lift coefficient occurs at lower spin ratio and thus the negative lift (i.e. inverse Magnus effect) starts to appear at lower spin ratio. The velocity field measured from a particle image velocimetry (PIV) indicates that the inverse Magnus effect results from the differences in the boundary-layer growth and separation along the retreating and advancing sphere surfaces: i.e., the main separation is delayed more on the advancing side than on the retreating side. The radius of curvature of streamlines on the advancing side becomes smaller than that on the retreating side, resulting in lower pressure on the advancing side. As a result, the lift force becomes negative with the wake deflected from advancing to retreating side.

INTRODUCTION

Flow over a rotating sphere is of a significant interest in many sports such as golf, baseball, tennis, table tennis, soccer, and volleyball, because all the balls used in these sports translate and rotate simultaneously. For a clockwise-rotating sphere moving from right to left, it is well known that the lift exerts an upward force, which is called the Magnus effect (Magnus, 1853). However, at some specific Reynolds numbers and spin ratios, the lift exerts in the opposite direction to the Magnus force, which is called the inverse (or negative) Magnus effect. Although several studies have experimentally measured the negative lift on a rotating sphere (Maccoll, 1928; Davies, 1949; Taneda, 1957; Briggs, 1959; Tanaka *et al.*, 1990; Aoki *et al.*, 2003*a*,*b*; Barlow & Domanski, 2008; Kray *et al.*, 2012), no quantitative velocity measurement has been performed to understand this phenomenon. Therefore, in the present study, we experimentally investigate the mechanism of the inverse Magnus effect on a rotating sphere through direct measurements of drag and lift forces and measurement of velocity using a PIV.

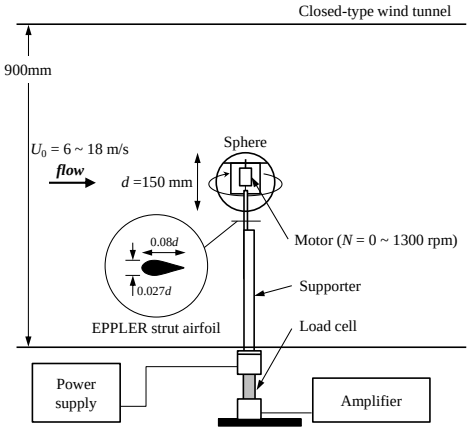

Figure 1. Experimental set-up for force measurement.

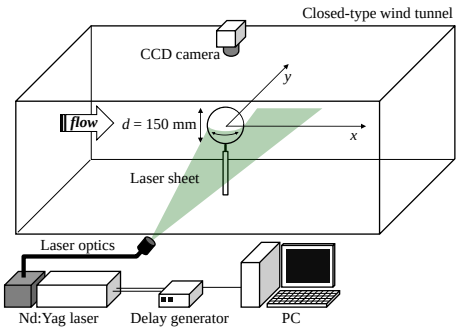

Figure 2. Experimental set-up for PIV measurement.

EXPERIMENTAL SETUP

Figure 1 shows the schematic diagram of the present experimental set-up for force measurement, consisting of a sphere, motor, supporter, load cell, and a closed-type wind tunnel. The cross-section of the wind tunnel after contraction is 900 mm × 900 mm and the turbulence intensity is lower than 0.3% at the free-stream velocity of 20 m/s. A sphere of 150 mm diameter is made of ABS resin. The blockage ratio of the cross-sectional area of sphere to the test-section area is about 2%, which is below the critical value ensuring negligible blockage effect on the flow field according to Achenbach (1974). A motor is installed inside the sphere and rotates it about the vertical axis. The sphere with motor is fixed to the supporter whose cross section is EPPLER strut airfoil. The three-dimensional forces are measured by three load cells (one BCL-3L and two LCB 03s) attached to the supporter. The measured forces are corrected by subtracting those of isolated supporter measured separately. The rotational speed of the sphere is measured by using a tachometer. The free-stream velocity U_0 varies from 6 to 18 m/s, corresponding to the Reynolds numbers, $Re = U_0 d/\nu = 0.6 \times 10^5 - 1.8 \times 10^5$, where ν is the kinematic viscosity. The rotational speed N varies from 0 (no spin) to 1300 rpm, corresponding to the spin ratios, $\alpha = \pi dN/60U_0 = 0 - 1.7$.

Figure 2 shows the schematic diagram for measuring velocity field behind a rotating sphere using two-component PIV. The PIV system consists of a Nd:Yag laser of 120 mJ, a CCD camera of 2048 × 2048 pixels resolution and a delay generator. A 60 mm lens is equipped with the camera to provide a field-of-view (FoV), whose dimensions are 160 mm × 160 mm on a streamwise center plane parallel to the mean flow and normal to the axis of rotation. 8 FoVs are used to cover the velocity field of $-0.6 < x/d < 2.5$ and $-1 < y/d < 1$ in the present experiment. Here, the velocity is measured with rotating the sphere both in the clockwise and counter-clockwise directions, so there exists no any shaded region in the whole velocity field. Iterative cross-correlation analysis is performed with an initial window size of 64 × 64 pixels and with 32 × 32 final interrogation windows. The interrogation window is overlapped by 50%, leading to a spatial resolution of $0.0086d$.

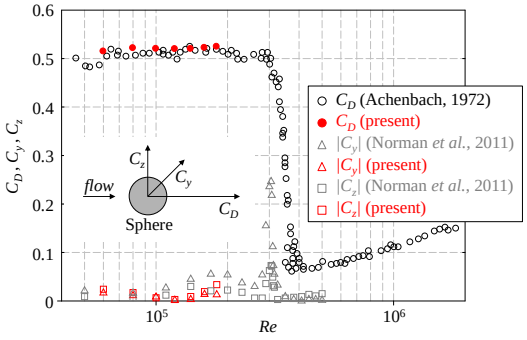

Figure 3. Variations of force coefficients on a stationary sphere with the Reynolds number.

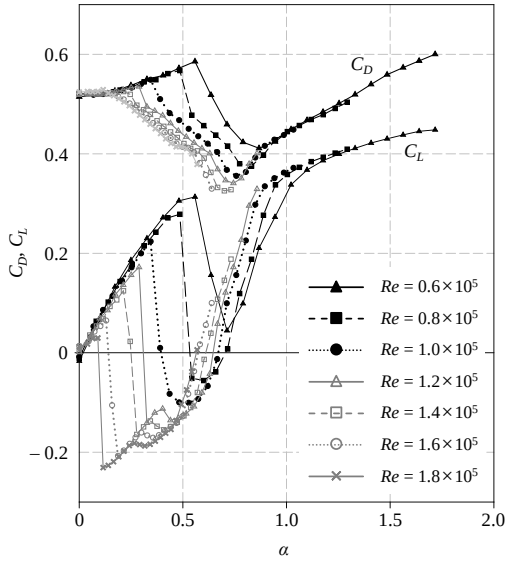

Figure 4. Variations of the lift and drag coefficients on a rotating sphere with the spin ratio.

RESULTS AND DISCUSSION

Force measurement

To investigate the extent of support interference, the force coefficients C_D, C_y and C_z on a non-rotating sphere are measured and compared to those of previous experimental studies (Figure 3). In the present study, a sphere is fixed to the crossflow supporter to rotate the sphere, whereas Achenbach (1972) and Norman *et al.* (2011) supported a

non-rotating sphere from rear side to minimize the support interference. As shown in Figure 3, the present results show good agreements with those with rear supports, ensuring negligible support interference from our study.

Figure 4 shows the variations of the lift and drag coefficients on a rotating sphere with the spin ratio at $Re = 0.6 \times 10^5 - 1.8 \times 10^5$. Note that the lift coefficient is defined as positive when the lift force exerts from the advancing to the retreating side (i.e. Magnus effect occurs) and vice-versa. At a given Re, the lift coefficient almost linearly increases in the positive direction with increasing spin ratio. However, with further increasing α, the lift coefficient rapidly decreases and then becomes negative. At higher Reynolds number, the lift coefficient shows rapid fall-off at lower spin ratio and thus the negative lift (i.e. inverse Magnus effect) starts to appear at lower spin ratio. After the lift coefficient reaches minimum, it increases and then becomes positive again. The spin ratio for return to positive lift force also decreases with increasing Reynolds number.

At a given Re, the behavior of the drag coefficient is quite similar to that of the lift coefficient, in that it increases with the spin ratio, then suddenly falls off, and then increases again. The drag coefficient starts to decrease at the same spin ratio where the lift coefficient shows fall-off, but to increase at higher α as compared to the lift coefficient.

Velocity measurement

To investigate the flow characteristics over a rotating sphere associated with the Magnus and inverse Magnus effects, we measure the velocity fields using a PIV. The experimental conditions for the velocity measurement and the corresponding lift and drag coefficients are shown in Table 1.

Table 1. Experimental conditions for the velocity measurement and the corresponding lift and drag coefficients.

Case	Re	α	C_L	C_D
a	1.0×10^5	0	0.05	0.52
b	1.0×10^5	0.34	0.22	0.55
c	1.0×10^5	0.53	-0.10	0.45
d	1.0×10^5	0.8	0.23	0.36

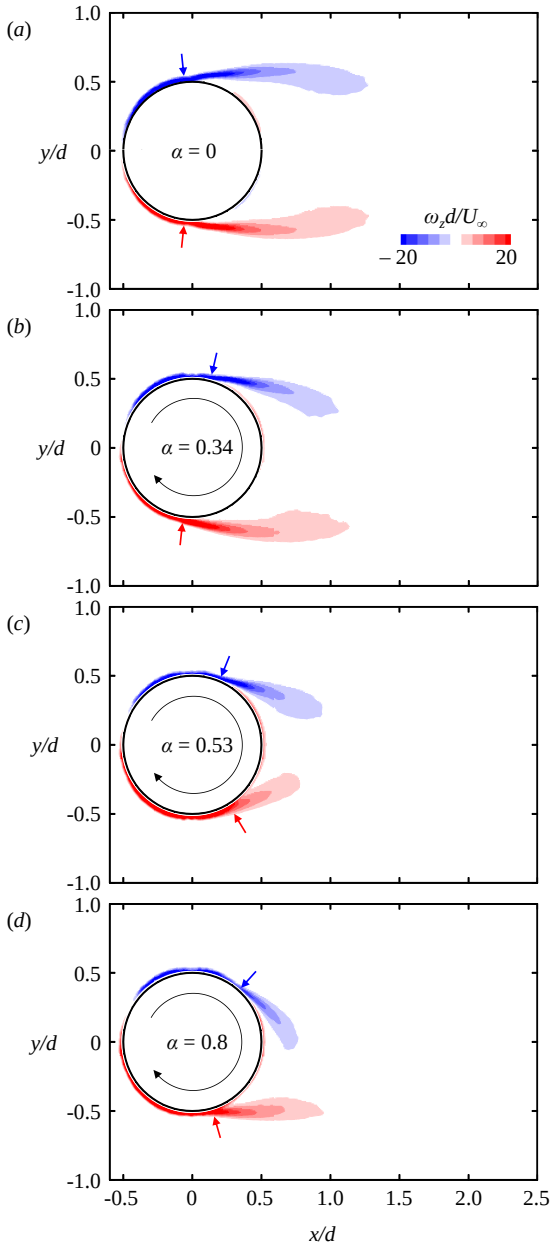

Figure 5. Contours of the mean azimuthal vorticity at $Re = 1.0 \times 10^5$ for (a) $\alpha = 0$ (no spin); (b) $\alpha = 0.34$; (c) $\alpha = 0.53$; (d) $\alpha = 0.8$. Note that the blue and red arrows indicate the positions of boundary-layer separation on the retreating and advancing sides, respectively.

Figures 5 and 6 shows the contours of mean azimuthal vorticity and time-averaged streamlines, respectively. Note that the blue and red arrows in Figure 5 indicate the positions of boundary-layer separation on the retreating and advancing sides, respectively. For rotating spheres, the position of flow separation is determined by MRS criterion ($u_\theta = 0$ and $\partial u_\theta / \partial r = 0$, where (r, θ) are the polar coordinates with the origin at the center of a sphere) proposed by Moore (1958), Rott (1956), and Sears (1956). Without the rotation ($\alpha = 0$), the flow separation occurs at $\theta \approx 84^\circ$ (Figure 5a), where θ is the azimuthal angle from the stagnation point. With increasing the spin ratio to 0.34, the rotation moves the separation point upstream on the advancing and downstream on the retreating side, as compared to those for a non-rotating sphere (Figure 5b). Therefore, the radius of curvature R of the streamlines becomes smaller on the retreating side than on the advancing side (Figure 6b). The smaller R on the retreating side means larger normal pressure gradient from the ambient pressure by the relation $\partial p / \partial n = -\rho V^2 / R$, where n is the local normal direction to the streamline and V is the local flow speed. The pressure is smaller on the retreating side than on the advancing side as a result of larger normal pressure gradient on the retreating side, leading to an upward (or positive) lift force (see Table 1). As shown in Figure 6b, the wake is deflected downwards with the positive lift force. However, at $\alpha = 0.53$, high shear rate on the advancing side causes earlier boundary-layer transition, resulting in the separation delay. Therefore, the main separation is delayed further downstream on the

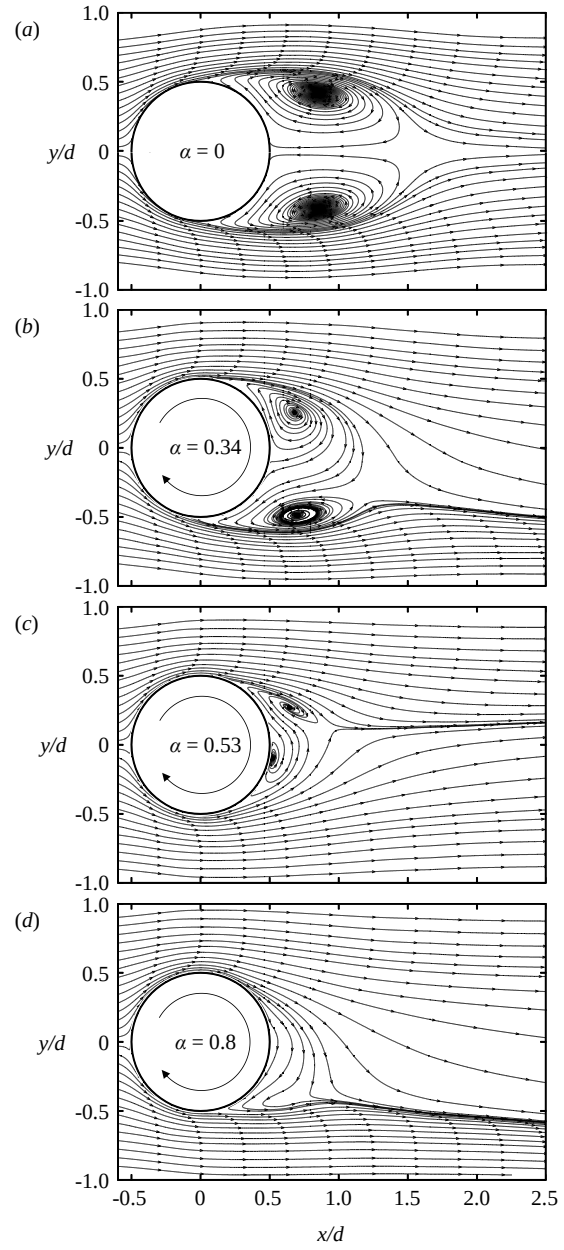

Figure 6. Time-averaged streamlines at $Re = 1.0 \times 10^5$ for (a) $\alpha = 0$ (no spin); (b) $\alpha = 0.34$; (c) $\alpha = 0.53$; (d) $\alpha = 0.8$.

advancing side than on the retreating side (Figure 5*c*). The pressure is smaller on the advancing side due to the delayed flow separation, resulting in the downward (negative) lift force (see Table 1). The wake is deflected upwards with the negative lift force as shown in Figure 6*c*. Note that the separation delay on the advancing and retreating side shrinks the recirculation zone behind the sphere, and thus the drag coefficient decreases (see Table 1). With further increasing the spin ratio to 0.8, the boundary-layer transition moves upstream with the increased velocity shear rate on the advancing side, and thus the main separation point moves upstream (Figure 5*d*). On the other hand, the rotation keeps delaying the separation point on the retreating side, resulting in the return to the positive lift force (see Table 1). As shown in Figure 6*d*, the wake is deflected downwards again, together with the positive lift force.

CONCLUSION

In the present study, the inverse Magnus effect on a rotating sphere was experimentally investigated at $Re = 0.6 \times 10^5 - 1.8 \times 10^5$ and $\alpha = 0 - 1.7$. At a given Re, the lift coefficient increased with the spin ratio at low α (thus showing the Magnus effect), but rapidly fell to negative (i.e. inverse Magnus effect occurred) at a certain spin ratio, and then increased again to a positive value. At higher Reynolds number, the lift coefficient showed rapid fall-off at lower spin ratio and thus the inverse Magnus effect started to appear at lower spin ratio. The behavior of the drag coefficient was quite similar to that of the lift coefficient, in that it increased with the spin ratio, then suddenly fell off, and then increased again. The velocity field measured from a PIV indicated that the inverse Magnus effect resulted from the differences in the boundary-layer growth and separation along the retreating and advancing sphere surfaces. That is, the main separation was delayed more on the advancing side than on the retreating side. The radius of curvature of the streamlines on the advancing side became smaller than that on the retreating side, resulting in the smaller pressure on the advancing side. As a result, the lift force became negative with the wake deflected from advancing to retreating side.

REFERENCES

Achenbach, E. 1972 Experiments on the flow past spheres at very high reynolds numbers. *Journal of Fluid Mechanics* **54** (3), 565–575.

Achenbach, E. 1974 The effects of surface roughness and tunnel blockage on the flow past spheres. *Journal of fluid mechanics* **65** (1), 113–125.

Aoki, K., Kinoshita, Y., Nagase, J. & Nakayama, Y. 2003*a* Dependence of aerodynamic characteristics and flow pattern on surface structure of a baseball. *Journal of visualization* **6** (2), 185–193.

Aoki, K., Ohike, A., Yamaguchi, K. & Nakayama, Y. 2003*b* Flying characteristics and flow pattern of a sphere with dimples. *Journal of visualization* **6** (1), 67–76.

Barlow, J.B. & Domanski, M.J. 2008 Lift on stationary and rotating spheres under varying flow and surface conditions. *AIAA journal* **46** (8), 1932–1936.

Briggs, L.J. 1959 Effect of spin and speed on the lateral deflection (curve) of a baseball; and the magnus effect for smooth spheres. *American Journal of Physics* **27** (8), 589–596.

Davies, J.M. 1949 The aerodynamics of golf balls. *Journal of Applied Physics* **20** (9), 821–828.

Kray, T., Franke, J. & Frank, W. 2012 Magnus effect on a rotating sphere at high reynolds numbers. *Journal of Wind Engineering and Industrial Aerodynamics* **110**, 1–9.

Maccoll, J.W. 1928 Aerodynamics of a spinning sphere. *Journal of the Royal Aeronautical Society* **28**, 777–798.

Magnus, G. 1853 Ueber die abweichung der geschosse, und: Ueber eine auffallende erscheinung bei rotirenden körpern. *Annalen der Physik* **164** (1), 1–29.

Moore, F.K. 1958 On the separation of the unsteady laminar boundary layer. *Boundary Layer Research, H. G. Görtler, ed., Springer, Berlin* pp. 296–311.

Norman, AK, Kerrigan, EC & McKeon, BJ 2011 The effect of small-amplitude time-dependent changes to the surface morphology of a sphere. *Journal of Fluid Mechanics* **675**, 268–296.

Rott, N. 1956 Unsteady viscous flow in the vicinity of a stagnation point. *Quarterly of Applied Mathematics* **13** (4), 444–451.

Sears, WR 1956 Some recent developments in airfoil theory. *Journal of Aeronautical Science* **23** (5), 490–499.

Tanaka, T., Yamagata, K. & Tsuji, Y. 1990 Experiment of fluid forces on a rotating sphere and spheroid. In *Proc. of the 2nd KSME-JSME Fluids Engineering Conference, Seoul, Korea, October*, pp. 10–13.

Taneda, S. 1957 Negative magnus effect. *Reports of Research Institute for Applied Mechanics* **5** (20), 123–128.